Low-loss ARROW waveguide with rectangular hollow core and rectangular low-density polyethylene/air reflectors for terahertz waves

Henri P. Uranus
Department of Electrical Engineering, Universitas Pelita Harapan, Jl. M. H. Thamrin 1100, Tangerang 15811, Indonesia.
henri.uranus@uph.edu

B. M. A. Rahman
Department of Electrical & Electronic Engineering, City, University of London, Northampton Square, London EC1V 0HB, United Kingdom.
E-mail: b.m.a.rahman@city.ac.uk

Received, Day Month Year

Designing low-loss waveguides for terahertz waves is challenging as most materials are very lossy in this frequency band. Most scientists simply consider transmitting the waves through low-loss air, which however also has its own difficulties as index-guiding is not possible. In this paper, we report on the design of low-loss waveguides for terahertz waves and associated results by using a finite element leaky mode solver. These results show that waveguides designed using ARROW (anti-resonant reflecting optical waveguide) approach yield a low combined absorption and leakage loss down to only 0.05 dB/cm for the q-TE_{00} fundamental mode using realistic values of refractive index at 1 THz operating frequency. The structure employs rectangular hollow-core and low-density polyethylene/air anti-resonant reflecting bilayers, which can be easily fabricated. These results are compared with those of other structures, i.e. a photonic crystal fiber-like structures using the same materials with rectangular holes, which is shown to give a higher loss of 3 dB/cm and a suspended air-core waveguide with TOPAS vein offering a loss of 1 dB/cm.

Keywords: Terahertz waves; terahertz waveguides; finite element method; hollow-core waveguide; anti-resonant reflecting optical waveguide; ARROW; mode solver; leaky modes.

1. Introduction

Terahertz (THz) waves[1] or T-rays are electromagnetic waves located in a spectrum gap between the optics and microwave bands, loosely defined as radiation from 0.1 THz (wavelength 3 mm) to 10 THz (wavelength 30 μm). On the other hand, it has also been defined as millimeter waves in the band from 0.3 THz (wavelength 1 mm) to 3 THz (wavelength 0.1 mm).

Terahertz waves applications include spectroscopy for material characterization, astronomy, imaging, and biosensor[1] due to its photon energy that fits well to vibrational and rotational transition of many molecular cluster. As a non-ionizing radiation, terahertz waves also find applications in imaging of inner layer of fragile archaeological ancient artworks[2] and even has been applied to human for full-body scanner[3] for airport security. The availability of high power THz sources open door to nonlinear optics and nonlinear spectroscopy in terahertz regime.[4] Four wave mixing nonlinear effect was also employed for THz generation in fiber.[5] Terahertz waves was also proposed for enhancement of harmonic yield of high harmonic generator for producing attosecond XUV and X-ray pulse.[6] For developing terahertz system, sources and detectors are not the only components. Terahertz absorbers,[7] modulators,[8] splitters,[8] waveguides,[5,9] planar circuits,[8] etc. were recently reported. In fact, a component that plays role as the basic building block for terahertz system is a waveguide.

Optical waveguides are usually designed for working wavelength in the vicinity of infrared wavelengths, around 1 μm, and the resulting devices have sizes between hundreds of nm to few tens of μm. By considering wavelength scaling rules,[10] sizes of devices working in THz-waves will be roughly hundreds to thousands times larger than devices working in optical regime. This suggests that depending on working wavelength

and function, devices for THz regime will have size from tens of μm to few millimeters. Certainly, such larger size devices will be easier to realize by using simpler fabrication technologies within the reach of scientists in developing countries.

However, one of the major problems in developing such guided-wave devices, particularly waveguides for terahertz (THz) band, is that most materials are lossy in this frequency band. Polymers, metals, and semiconductors materials, all suffer from considerable loss in this THz regime. In order to circumvent this, most scientists have considered to guide the waves through the low-loss air within their waveguides, leading to hollow-core structures. However, such scheme has its own difficulties, as air has a low refractive index, hence index-guided waveguiding scheme is not possible and besides that both absorption loss and leakage loss[11] are also present. To deal with this, several schemes have been proposed, e.g. by putting metal wires[12] or metal coatings[13] as reflectors, by simply having the reflection from dielectric interfaces,[14] photonic crystal fiber (PCF)-like holey cladding,[15] anti-resonant reflection,[16] or using the legacy microwave structures like microstrip structures[17] and hollow-core metallic tube,[18] etc.

As a close neighbour, devices working in THz regime can also be modeled by using the similar modeling techniques usually used in optics. In this work, we have used a finite element-based leaky mode solver incorporating Bayliss-Gunzburger-Turkel-like transparent boundary conditions which has previously been applied for optics[19-20], for studying THz waveguides. The numerically simulated results show that a hollow-core structure designed with ARROW (anti-resonant reflecting optical waveguide) principles[21] with rectangular core and rectangular low-density polyethylene/air reflectors is promising as it yields a low attenuation constant. We have intentionally selected structures with rectangular cross-sectional features since this shape can be more easily fabricated by using relatively simple fabrication technologies, similar to technologies that we have developed for fabricating microfluidic structures[22], where patterned sheets are stacked and thermally bonded. Additionally, these structures support quasi-linearly polarized modes which makes coupling from terahertz sources easier.

2. Method being Used

For this work, we have used a finite-element method (FEM) based on vectorial leaky mode solver utilising the transverse **H**-field formulation incorporating Bayliss-Gunzburger-Turkel-like transparent boundary conditions (TBC). Detail explanations on the numerical scheme of the mode solver has been given in Refs. 19 and 20.

Since the structures are both leaky and lossy, both properties should be well incorporated into the model. The leaky property is taken into account by proper boundary conditions, which is already built-in in the solver through the TBC, while the lossy property is taken into account by considering the complex refractive index of the materials. Data of complex refractive index of the materials were obtained from data or curves given in published literatures.[23-25]

3. Design of the ARROW Waveguide

The proposed ARROW structure composed of low-density polyethylene (LDPE) with a hollow-core and holey cladding of rectangular shapes is shown in Fig. 1.

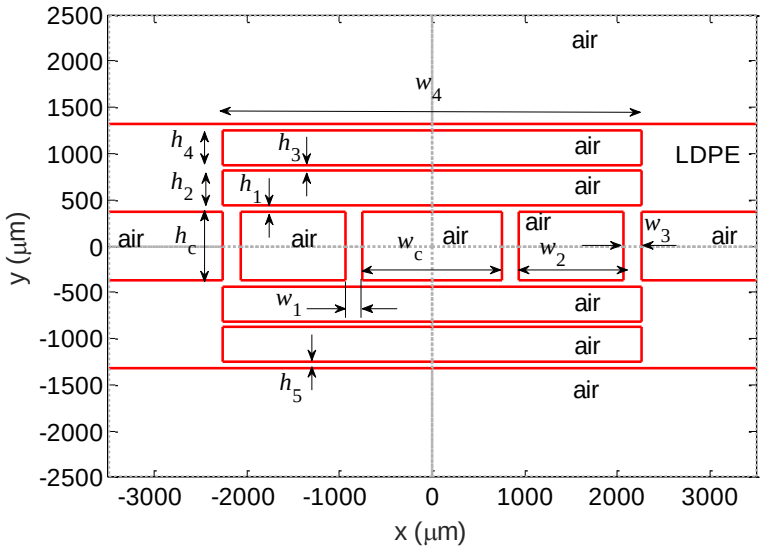

Fig. 1. The cross-section of the proposed ARROW waveguide structure.

3.1. Determining the core size

In order to confine the waves inside the core, a resonant condition was imposed by choosing a proper size, which is both achievable by available fabrication technology and also resonant. To simplify the numerical analyses, we have reduced the structure to a planar system as illustrated in Fig. 2. It should be noted that due to such reduction, the approach is approximative, however, very useful for a quick design.

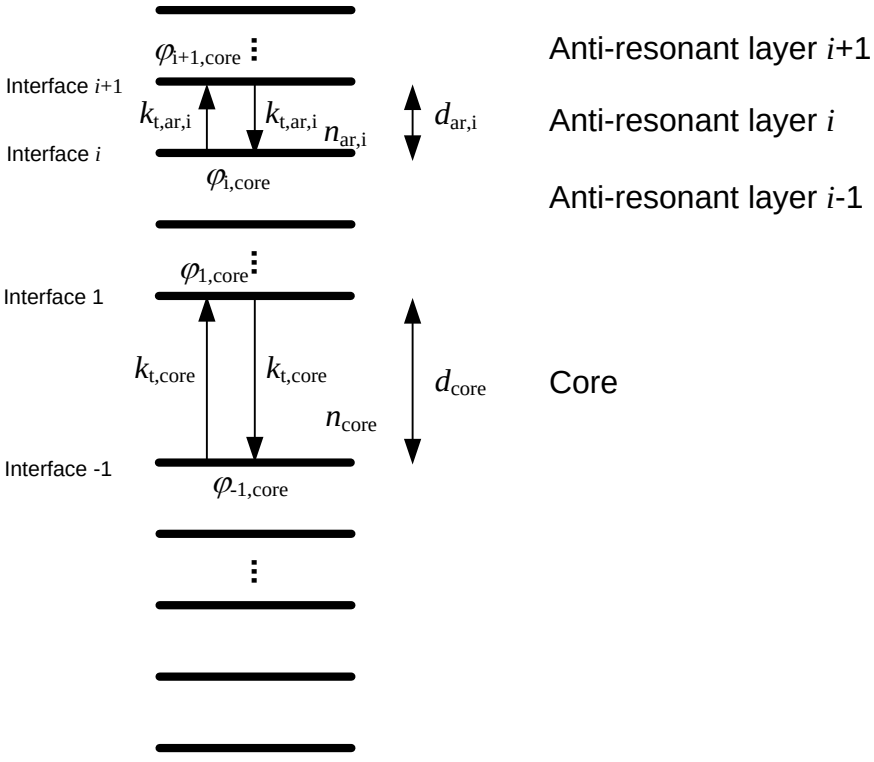

Fig. 2. The round-trip of the transverse waves in the core and the anti-resonant reflecting layers.

For this, the transverse resonance condition requires that the round trip phase change in the core, as illustrated in Fig. 2, should be multiple of 2π, which leads to

$$2k_{\mathrm{t,core}}d_{\mathrm{core}} - \varphi_{1,\mathrm{core}} - \varphi_{-1,\mathrm{core}} = 2\pi M_{\mathrm{core}} \tag{1}$$

with $M_{\mathrm{core}} = \{1, 2, 3, \ldots\}$, and $k_{\mathrm{t,core}}$, d_{core}, $\varphi_{1,\mathrm{core}}$ and $\varphi_{-1,\mathrm{core}}$ are the transverse wave vector in the core, thickness (wide or height) of the core, and phase shift due to reflection at the interfaces 1 and -1, respectively. It should be noted that the negative sign of the phase comes from choice of positive frequency, where $E = E_0 exp(i\omega t - i\beta L)$ representing wave moving towards the positive L direction. Figure 2 suggests that

$$k_{\mathrm{t,core}} = k_0 \mathrm{Re}\left[\sqrt{n_{\mathrm{core}}^2 - n_{\mathrm{eff}}^2}\right] \tag{2}$$

with $k_0 = 2\pi/\lambda$, n_{core}, n_{eff}, and λ, representing the vacuum wavenumber, core refractive index, mode effective index, and electromagnetic wavelength, respectively. Notation "Re[]" denotes the real part of a complex quantity. Substituting Eq. (2) into Eq. (1) gives

$$d_{\mathrm{core}} = \frac{2M_{\mathrm{core}} + \frac{\varphi_{1,\mathrm{core}} + \varphi_{-1,\mathrm{core}}}{\pi}}{4\mathrm{Re}\left[\sqrt{n_{\mathrm{core}}^2 - n_{\mathrm{eff}}^2}\right]}\lambda \tag{3}$$

with the phase shift due to reflection at interfaces 1 and -1 are given by

$$\varphi_{l,\mathrm{core}} = \mathrm{atan}\left\{\frac{\mathrm{Im}[r_{l,\mathrm{core}}]}{\mathrm{Re}[r_{l,\mathrm{core}}]}\right\} \tag{4}$$

with $l = \{1, -1\}$, "Im[]" denotes the imaginary part of a complex quantity, and $r_{l,\mathrm{core}}$ is the reflection at interface l for electromagnetic radiation coming from core. These reflection coefficients for the TE and TM polarisations are given by[21]

$$r_{l,\mathrm{core,TE}} = \frac{k_{\mathrm{t,core}} - k_{\mathrm{t},l}}{k_{\mathrm{t,core}} + k_{\mathrm{t},l}} \tag{5}$$

$$r_{l,\mathrm{core,TM}} = \frac{n_l^2 k_{\mathrm{t,core}} - n_{\mathrm{core}}^2 k_{\mathrm{t},l}}{n_l^2 k_{\mathrm{t,core}} + n_{\mathrm{core}}^2 k_{\mathrm{t},l}} \tag{6}$$

with $k_{\mathrm{t},l}$ representing the transverse wave vector in the cladding layer next to interface l, while n_l is the refractive index of cladding next to interface l.

3.2. Determining the anti-resonant reflection cladding size

For the waves to be confined inside the core, we need to impose the antiresonant condition in each of the cladding reflecting layers. To simplify the analyses, we again reduce the system into 1-D problem, as illustrated in Fig. 2.

The antiresonance condition requires that the round trip phase change in each of the reflecting cladding layer should be odd multiple of π, which leads to

$$2k_{\mathrm{t,ar},i}d_{\mathrm{ar},i} - \varphi_{i,\mathrm{ar}} - \varphi_{i+1,\mathrm{ar}} = 2\pi\left(M_{\mathrm{ar}} + \frac{1}{2}\right) \tag{7}$$

with $M_{\mathrm{ar}} = \{0, 1, 2, \ldots\}$, while $k_{\mathrm{t,ar},i}$, $d_{\mathrm{ar},i}$, $\varphi_{i,\mathrm{ar}}$ and $\varphi_{i+1,\mathrm{ar}}$ are the transverse wavenumber in the anti resonant layer i, thickness of the antiresonant layer i, and phase shifts due to reflection at interfaces i and i+1, respectively. By taking

$$k_{\mathrm{t,ar},i} = k_0 \mathrm{Re}\left[\sqrt{n_{\mathrm{ar},i}^2 - n_{\mathrm{eff}}^2}\right] \tag{8}$$

with $n_{\mathrm{ar},i}$ is the refractive index of the antiresonant layer i, substituting Eq. (8) into Eq. (7) gives the required thickness of the antiresonant layer i

$$d_{\mathrm{ar},i} = \frac{2M_{\mathrm{ar}} + 1 + \frac{\varphi_{i,\mathrm{ar}} + \varphi_{i+1,\mathrm{ar}}}{\pi}}{4\mathrm{Re}\left[\sqrt{n_{\mathrm{ar},i}^2 - n_{\mathrm{eff}}^2}\right]}\lambda \tag{9}$$

with phase shift at reflection at interface i and i+1 are given by

$$\varphi_{i,\mathrm{ar}} = \mathrm{atan}\left\{\frac{\mathrm{Im}[r_{i,\mathrm{ar}}]}{\mathrm{Re}[r_{i,\mathrm{ar}}]}\right\} \tag{9}$$

$$\varphi_{i+1,\mathrm{ar}} = \mathrm{atan}\left\{\frac{\mathrm{Im}[r_{i+1,\mathrm{ar}}]}{\mathrm{Re}[r_{i+1,\mathrm{ar}}]}\right\} \tag{10}$$

with $r_{i,\mathrm{ar}}$ is the reflection at interface i for electromagnetic waves coming from the antiresonant reflecting layer i toward i-1, r_{i+1} is the reflection at interface i+1 for waves coming from anti-resonant layer i toward i+1. These reflection coefficients for the TE and TM[21] polarisations are given by

$$r_{i,\mathrm{ar,TE}} = \frac{k_{\mathrm{t,ar},i} - k_{\mathrm{t,ar},i-1}}{k_{\mathrm{t,ar},i} + k_{\mathrm{t,ar},i-1}} \tag{11}$$

$$r_{i,\mathrm{ar,TM}} = \frac{n_{\mathrm{ar},i-1}^2 k_{\mathrm{t,ar},i} - n_{\mathrm{ar},i}^2 k_{\mathrm{t,ar},i-1}}{n_{\mathrm{ar},i-1}^2 k_{\mathrm{t,ar},i} + n_{\mathrm{ar},i}^2 k_{\mathrm{t,ar},i-1}} \tag{12}$$

$$r_{i+1,\mathrm{ar,TE}} = \frac{k_{\mathrm{t,ar},i} - k_{\mathrm{t,ar},i+1}}{k_{\mathrm{t,ar},i} + k_{\mathrm{t,ar},i+1}} \tag{13}$$

$$r_{i+1,\mathrm{ar,TM}} = \frac{n_{\mathrm{ar},i+1}^2 k_{\mathrm{t,ar},i} - n_{\mathrm{ar},i}^2 k_{\mathrm{t,ar},i+1}}{n_{\mathrm{ar},i+1}^2 k_{\mathrm{t,ar},i} + n_{\mathrm{ar},i}^2 k_{\mathrm{t,ar},i+1}} \tag{14}$$

For i=1, the refractive index of the core is used for $n_{\mathrm{ar},i\text{-}1}$ and the transverse wavenumber in core is used for $k_{\mathrm{t,ar},i\text{-}1}$.

3.3. For low-loss quasi-TE mode

For low-loss quasi-TE mode, we expect the **E**-field to be parallel to the lateral x-axis of the structure and **H**-field directed in the vertical y-direction as illustrated in Fig. 3. By observing the waveguide in Fig. 3 from *A-A'* cut, it shows that we will need core and anti-resonant layers to be optimized for TM polarization in the lateral direction as shown in Fig. 4(a). On the other hand, looking through the *B-B'* cut, it shows that the core and anti-resonant layers need to be optimized for TE polarization in the vertical direction, as shown in Fig. 4(b).

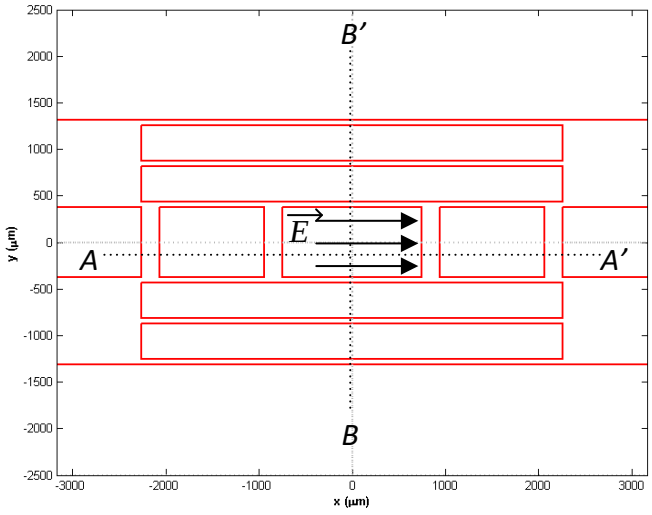

Fig. 3. Illustration on the waveguide optimized for low-loss quasi-TE mode guiding

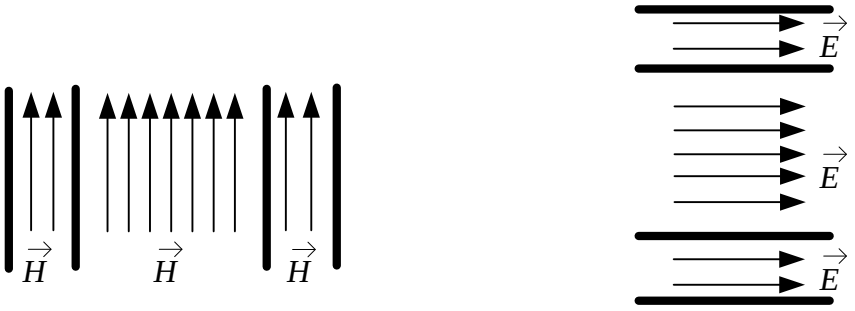

(a) (b)

Fig. 4. Illustration on the field directions, (a) TM polarization in lateral, and (b) TE polarization in the vertical directions, required for low-loss quasi-TE mode guiding

3.4. For low-loss quasi-TM mode

Similarly, for a low-loss quasi-TM mode guiding, we expect the **E**-field to be parallel to the vertical axis and **H**-field to be in the lateral direction, as shown in Fig. 5. Looking at the waveguide in Fig. 5 from *A-A'* cut, it shows that we will need core and antiresonant layers optimized for TE polarization in lateral direction as shown in Fig. 6(a). Meanwhile, looking through *B-B'* cut, it shows that we will need core and antiresonant layers optimized for TM polarization in vertical direction as shown in Fig. 6(b).

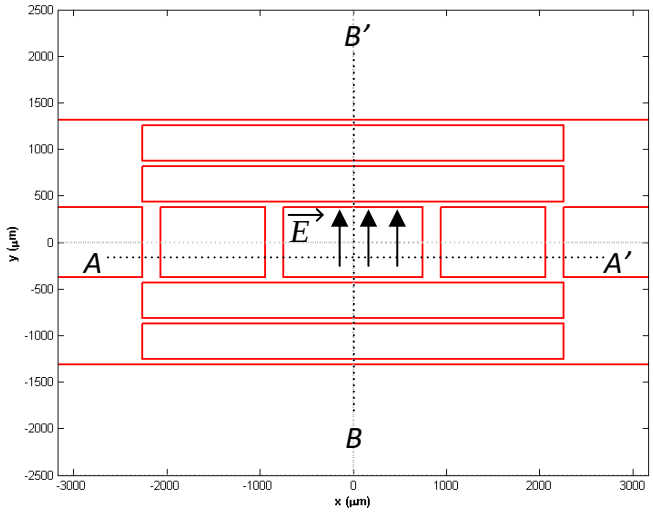

Fig. 5. Illustration on the waveguide optimized for low-loss quasi-TM mode guiding

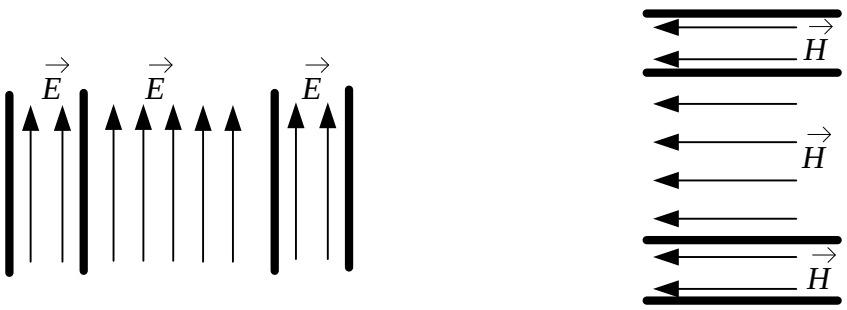

(a) (b)

Fig. 6. Illustration on (a). TE polarization in lateral, and (b). TM polarization in vertical direction required for low-loss quasi-TM mode guiding

3.5 Design of low-loss hollow-core ARROW

As discussed in Ref. 21, besides thickness of the antiresonant layers, selection of materials are also important for low-loss hollow-core with rectangular core due to the existence of Brewster's condition in TM reflection, and high index contrast for high reflection rule of thumb does not apply for TM reflection. The extrema of the TM reflection curve will be located at a point where one of the material has refractive index of $n = \sqrt{2}n_{\text{eff}}$. If we consider the n_{eff} value of 0.98, it will lead to a refractive index value of 1.39. Table 1 shows refractive indices of several polymers at 1 THz obtained from literatures.

Table 1. Refractive indices of several polymers at 1 THz

Name	Refractive index (n)	References
PTFE (Teflon)	1.445-i0.0047746	α=2 cm^{-1}, deduced from curve of Ref. 24
PS (polystyrene)	2.08-i0.003581	α=1.5 cm^{-1}, deduced from curve given in Ref. 25
HDPE (high density polyethylene)	1.54-i0.0007162	α=0.3 cm^{-1}, deduced from curve given in Ref. 25
LDPE (low density polyethylene)	1.54-i0.00066845	Re(n) taken from Ref. 23, Im(n) taken from loss model of Ref. 12

Table 2. Proper core size (width or height) of hollow-core ARROW with LDPE wall for n_{eff} = 0.98.

Order of resonance	Air core size (μm)	
M_{core}	TE polarization	TM polarization
1	1507.5	-
2	2261.27	753.8
3	3015.05	1507.6

Table 3. Proper thickness of antiresonant layers of hollow-core ARROW with LDPE/air bilayers for n_{eff} = 0.98.

Order of antiresonant	Antiresonant layer thickness (μm)			
	LDPE		Air	
M_{ar}	TE polarization	TM polarization	TE polarization	TM polarization
0	63.12	63.14	1130.61	-
1	189.39	189.41	1884.39	376.9
2	315.66	315.68	2638.16	1130.70

We have selected LDPE as its real part of refractive index is close to 1.39 and additionally also shows a lower material absorption value. Tables 2 and 3 show the proper core and reflecting layers sizes of air-core ARROW using LDPE/air reflecting layers in both vertical and lateral directions for several values of M_{core} and M_{ar} for n_{eff} = 0.98. Choosing M_{core}=2, M_{ar}=0 (for LDPE) and 1 (for air) gives core size of 753.8 μm and LDPE/air bilayer thickness of 63.14 μm/376.9 μm in vertical direction, and M_{core}=1 and M_{ar}=0 (for air) and 1 (for LDPE) gives core size of 1507.5 μm and LDPE/air bilayer thickness of 189.39 μm/1130.61 μm in lateral direction. Rounding up these values gives structure as shown in Fig. 1 with w_c=1500μm, h_c=750μm, h_1=h_3=h_5=63μm, h_2=h_4=376μm, w_1=w_3=190μm, w_2=1130μm, and w_4=4520μm. We should note that thinner LDPE in vertical direction and wider structures in lateral direction were intentionally chosen for the purpose of easier fabrication regarding sheet thickness limitation in thermal bonding method and sheet patterning resolution issues.[22]

4. Computational Results and Discussions

We employed the vectorial FEM leaky mode solver to evaluate the design. In the simulations using the FEM mode solver, the refractive index of air is taken as 1, while that of the LDPE is taken as 1.54-i*0.00066845 deduced from Refs. 4 and 23 at

1 THz operating frequency. Figures 7 and 8 show the q-TE_{00} (with prefix q denoting quasi) mode, which is the mode with lowest loss in this leaky and lossy structure. The loss of this mode is only 0.05 dB/cm. The longitudinal component of the time-averaged Poynting vector $<S_z(x,y)>$ clearly shows that the near-Gaussian shaped modal field is well confined inside the hollow-core. Taking advantage of available structural symmetry, the computation was performed only on a quarter of the structure with 15361 quadratic nodes with mesh distribution shown in Fig. 8. Figures 9 and 10 show results for the next lowest loss mode which is q-TM_{00} mode with α = 0.3 dB/cm. The loss of q-TE_{00} mode is 5.7 times lower in dB scale than the q-TM_{00} mode which will make the waveguide to be effectively single mode for a length of 80 cm with multimode rejection ratio (MMRR)[26] of 20 dB. We should note that the loss of q-TM mode is higher than q-TE because for q-TM mode, the TM reflections happen at interfaces in vertical stacks which the structure is thinner in size and also suffer from low reflection coefficients due to the Brewster's condition, hence the electromagnetic waves can easily leak away. The rectangular structure also induced quasi-linearly polarized modes which will be easy to couple from a terahertz source into the waveguide.

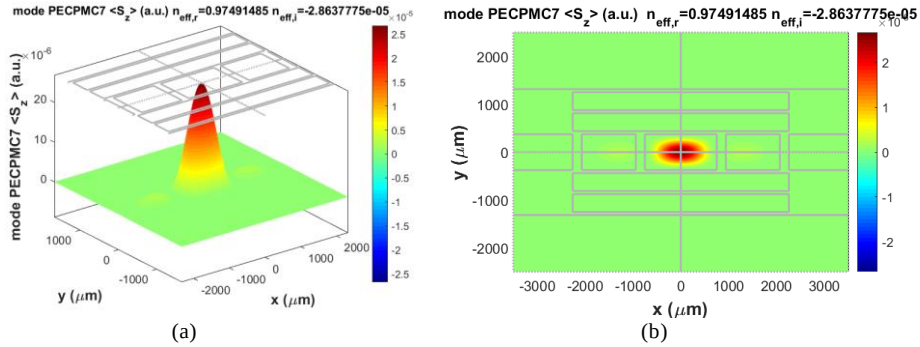

(a) (b)

Fig. 7. The longitudinal component of time-averaged Poynting vector of q-TE_{00} mode: (a) a 3-D profile with waveguide inset on top, and (b) its 2-D profile.

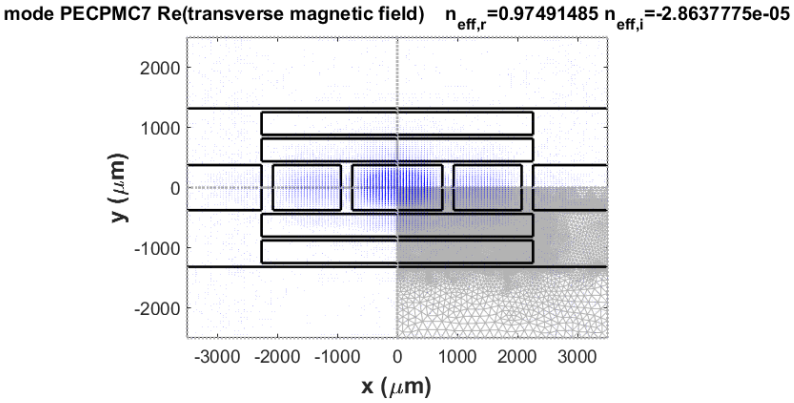

(a)

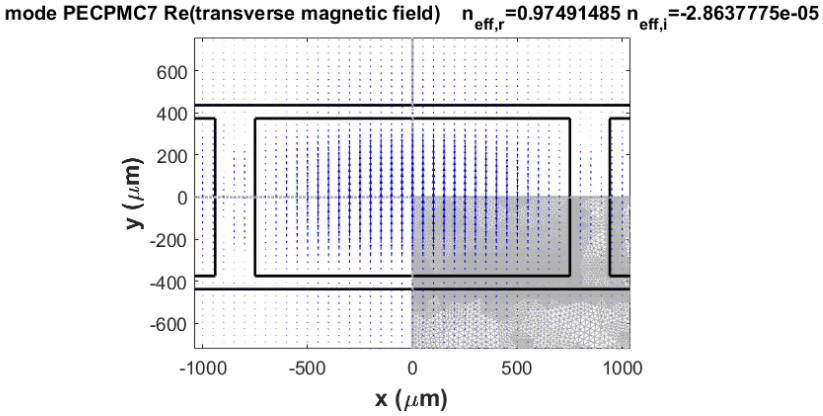

(b)

Fig. 8. (a) The transverse component of magnetic field vector ($\hat{x}H_x + \hat{y}H_y$) of q-TE_{00} mode and (b) its close-up distribution in the core.

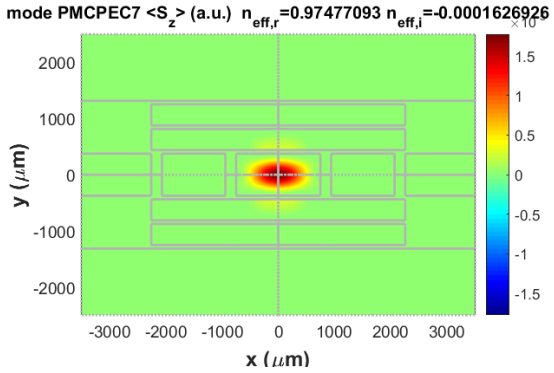

Fig. 9. The longitudinal component of time-averaged Poynting vector of q-TM_{00} mode

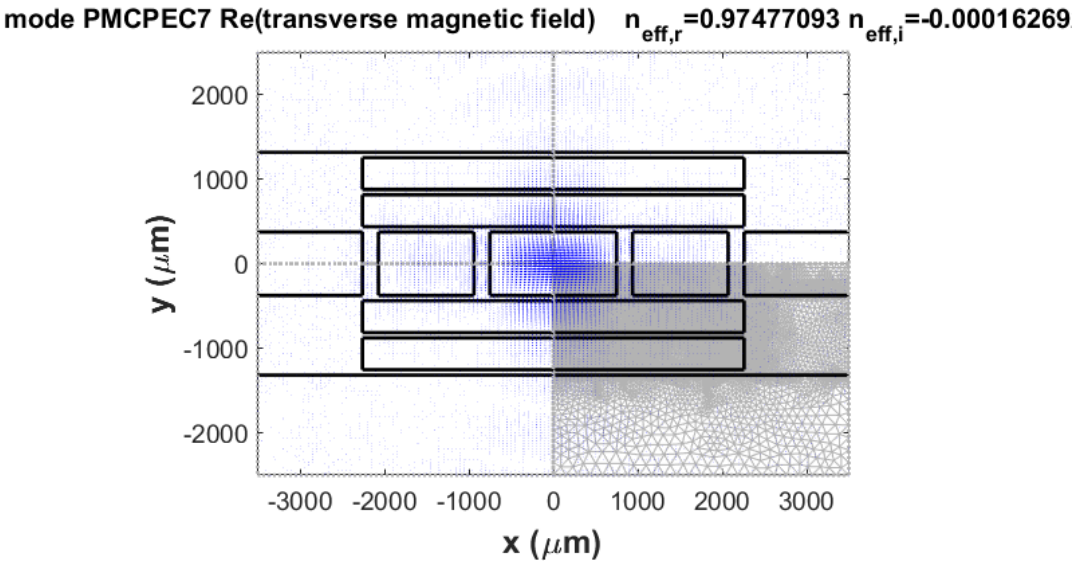

(a)

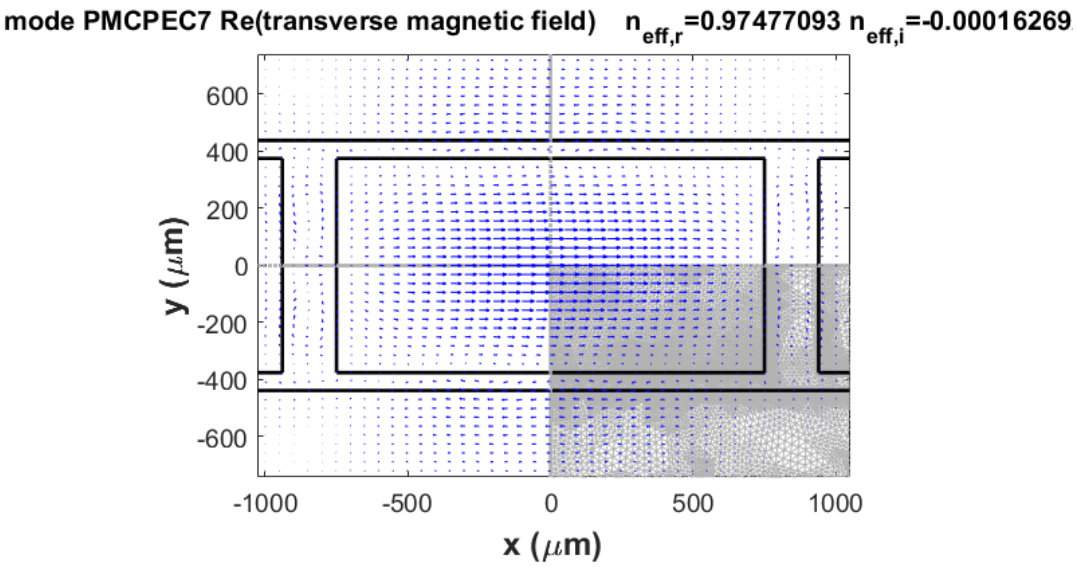

(b)

Fig. 10. (a) The transverse component of magnetic field vector ($\hat{x}H_x + \hat{y}H_y$) of q-TM_{00} mode and (b) its distribution in the core.

For comparison, we have also computed the modes of photonic crystal fiber-like (PCF-like) structure with same materials and of comparable size which we believe will share the same fabrication challenge as the ARROW structure, and a rather delicate suspended air-core waveguide with TOPAS vein.

The PCF-like structure with rectangular air-holes in LDPE is shown in Fig. 11. The numerically simulated results are shown in Fig. 12. The structure indeed shows a modal fields which are confined in the core, but since the core is lossy, it gives rather large loss of 3 dB/cm.

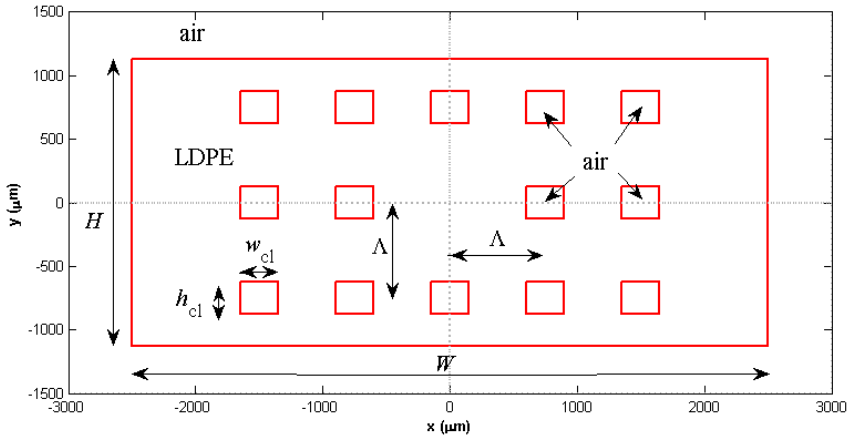

Fig. 11. Structure of a PCF-like waveguide with rectangular holes. W = 5000 μm, H = 2250 μm, w_{cl} = 300 μm, h_{cl} = 250 μm, pitch Λ = 750 μm.

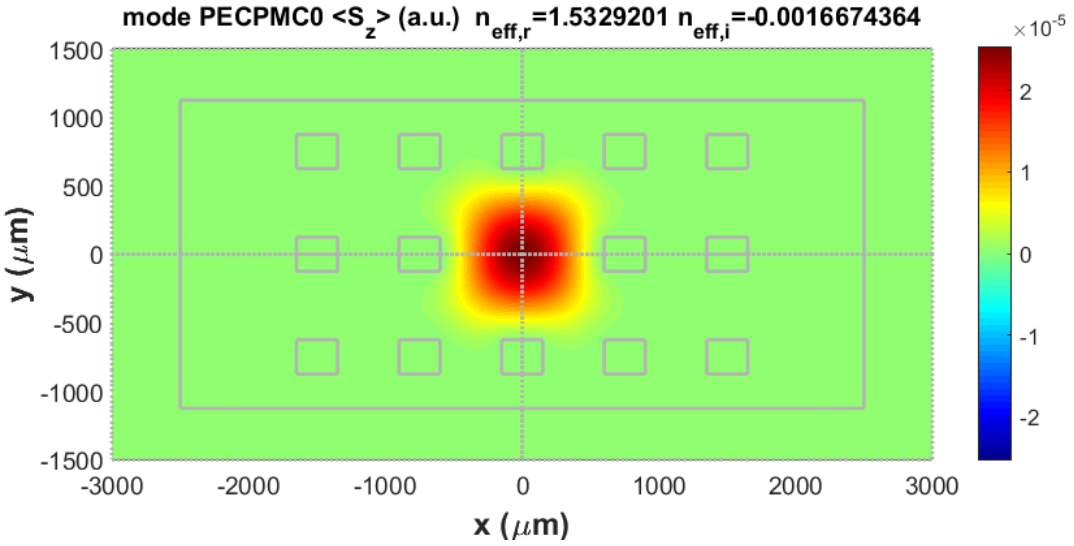

(a)

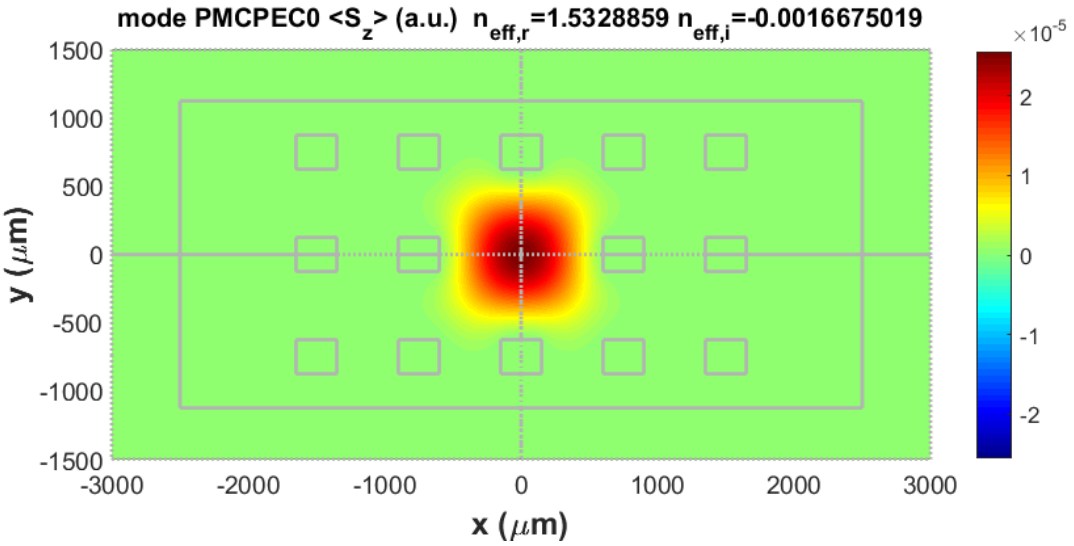

(b)

Fig. 12. The longitudinal component of time-averaged Poynting vector for modes of PCF-like structure using rectangular air holes within LDPE host (a) q-TE_{00}, α=3.033 dB/cm, and (b) q-TM_{00}, α=3.033 dB/cm.

The structure for a suspended square air-core with TOPAS (a nonpolar cyclic-olefin copolymer) vein was taken from Ref. 27. Although the structure is very delicate and hence would be difficult to fabricate, but due to the suspension, the core will be practically surrounded by low index air, hence is expected to give a rather low loss. The structure is shown in Fig. 13 with D = 4 mm, d = 20 μm, Λ = 100 μm, and t = 0.5 mm. The refractive index of air is taken to be 1 while for TOPAS is n = 1.5258 – i 0.0006589 (deduced from Ref. 27) for frequency of 1 THz. The results of the suspended air core structure are shown in Fig. 14. The q-TE_{00} core mode shows 1 dB/cm which is still higher than our proposed ARROW structure.

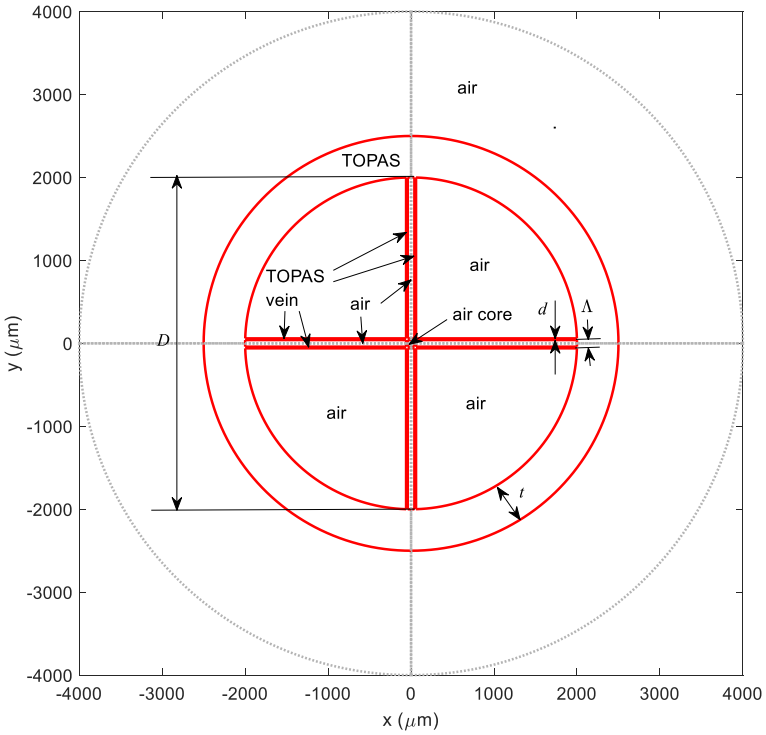

(a)

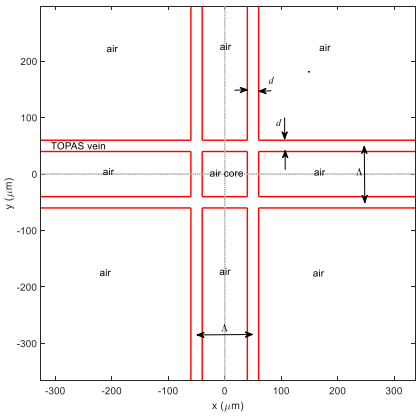

(b)

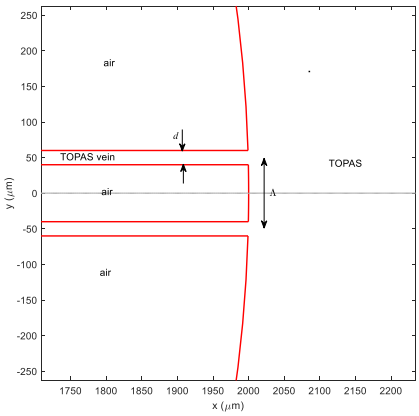

(c)

Fig. 13. The structure of suspended square air-core structure with TOPAS vein: (a) overall structure showing also the computational domain, (b) zoomed-in the core, and (c) zoomed-in the connection between the veins and the outer TOPAS shell.

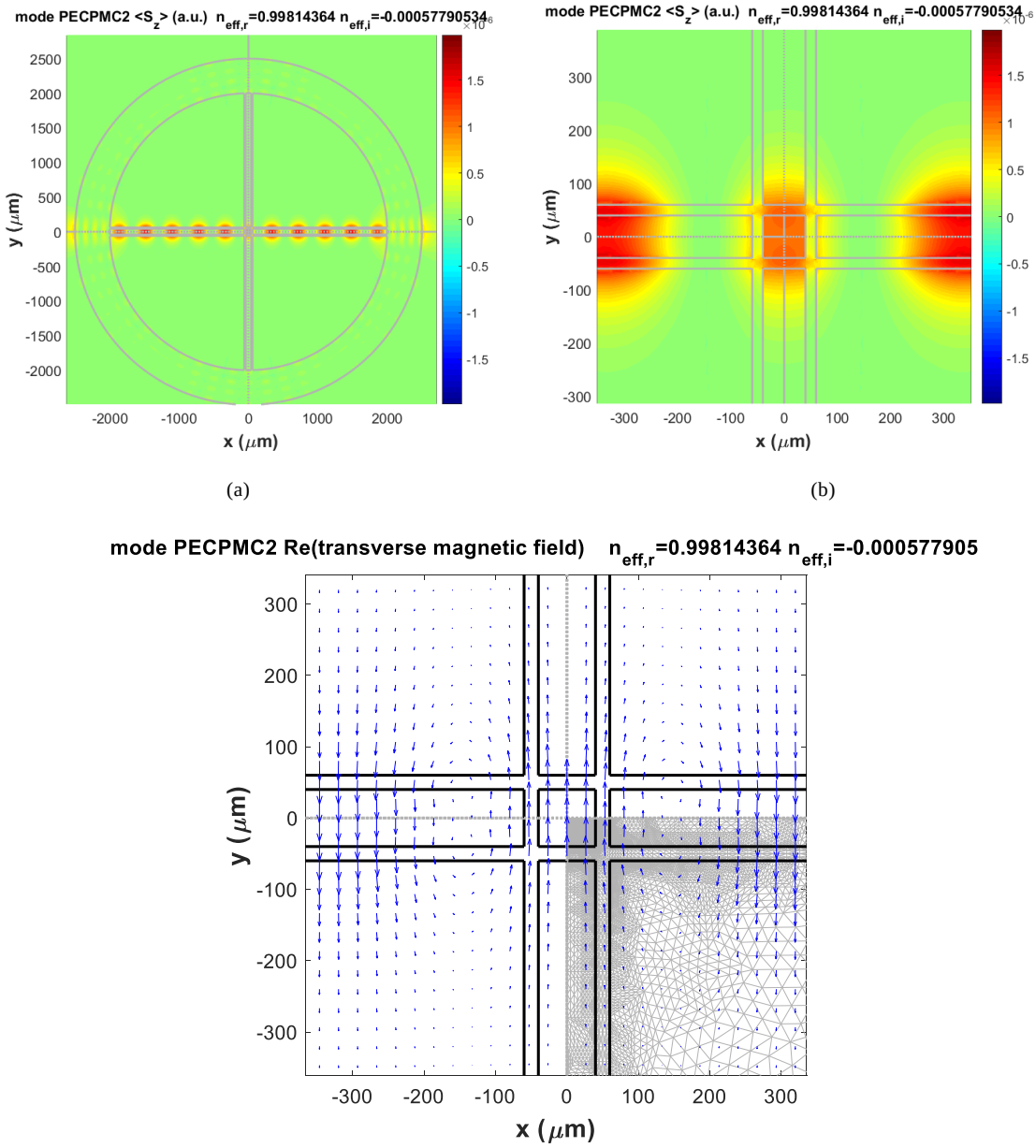

Fig. 14. The q-TE_{00} mode of the suspended air-core structure with TOPAS vein. (a) and (b) the longitudinal component of time-averaged Poynting vector, and (c). the transverse magnetic field vector around the core.

5. Conclusions

We proposed a hollow-core waveguide for terahertz waves exploiting the ARROW principles by using LDPE/air as the anti-resonant reflecting layers. The structure was designed with rectangular shapes which can be fabricated more easily by using simple manufacturing technology. The numerical simulations were carried out by using a finite element based leaky mode solver by taking into account the realistic complex refractive index of the materials. The results show that the proposed structure has a low loss value of 0.05 dB/cm, lower than those can be attained by PCF-like structure made of the same materials with comparable size, and the more complicated suspended air-core structure with TOPAS veins. By taking advantage of

the rectangular structure, the proposed waveguide supports quasi linearly polarized modes which will be easier to couple from terahertz sources.

Acknowledgment

This work was supported by Erasmus Mundus LEADERS mobility project financed by European Commission's EACEA grant number 2014-0855.

References

1. B. Ferguson and X. C. Zhang, Materials for terahertz science and technology. *Nature Materials* **1**(1) (2002) 26-33.
2. P. Daukantas, Cultural artifacts in terahertz light. *Opt. Photon. News* **29**(3) (2018) 28-35.
3. Terahertz security body scanner, http://terasense.com
4. J. Hebling, K. L. Yeh, M. C. Hoffmann, and K. A. Nelson, High-power THz generation, THz nonlinear optics, and THz nonlinear spectroscopy. *J. Sel. Topics in Quantum Elect.* **14**(2) (2008) 345-353.
5. A. Barh, B. P. Pal, G. P. Agrawal, R. K. Varsney, and B. M. A. Rahman, Specialty fiber for terahertz generation and transmission: A review. *J. Sel. Topics in Quantum Elect.* **2**(2) (2016) 365-379.
6. L. Feng, W. Li, R. S. Castle, Y. Li, High-intensity attosecond pulse generation by using inhomogeneous laser field in frequency and space. *J. Nonlinear Optical Phys. Mat.* **26**(3) (2017) 1750034-1 – 1750034-14.
7. H. L. Dang, V C Nguyen, D. H. Le, H. T. Nguyen, M. C. Tran, D. T. Le, D. L. Vu, Broadband metamaterial perfect absorber obtained by coupling effect. *J. Nonlinear Optical Phys. Mat.* **26**(3) (2017) 1750036-1-1750036-10.
8. A. S. Meijer, G. Berden, D. D. Arslanov, M. Ozerov, R. T. Jongma, W. J. van der Zande, An ultrawide-bandwidth single-sideband modulator for terahertz frequencies. *Nature Photon.* **10**(11) (2016) 740-744.
9. S. Atakaramians, S. Afshar V., T. M. Monro, and D. Abbott, Terahertz dielectric waveguides. *Adv. in Opt. and Photonics* **5**(2) (2013) 169-215.
10. J. D. Joannopoulos, S. G. Johnson, J. N. Winn, and R. D. Meade, *Photonic Crystals: Moulding the Flow of Light* (Princeton Univ. Press, 2008).
11. H. P. Uranus, *Guiding Light by and beyond the Total Internal Reflection Mechanism*, Ph.D. dissertation (Univ. Twente, 2005).
12. A. Markov and M. Skorobagatiy, Two-wire terahertz fibers with porous dielectric support. *Optics Express* **21**(10) (2013) 12728 – 12743.
13. C. Themistos, B. M. A. Rahman, M. Rajarajan, K. T. V. Grattan, B. Bowden, and J. A. Harrington, Characterization of silver/polystyrene (PS)-coated hollow glass waveguides at THz frequency. *J. Lightwave Technol.* **25**(9) (2009) 2456-2462.
14. D. Chen and H. Chen, A novel low-loss terahertz waveguide: Polymer tube. *Optics Express* **18**(4) (2010) 3762-3767.
15. M. Uthman, B. M. A. Rahman, N. Kejalakshmy, A. Agrawal, and K. T. V. Grattan, Design and characterization of low-loss porous-core photonic crystal fiber. *IEEE Photonics J.* **4**(6) (2012) 2315-2325.
16. C. H. Lai, B. You, J. Y. Lu, T. A. Liu, J. L. Peng, C. K. Sun, and H. C. Chang, Modal characteristics of antiresonant reflecting pipe waveguides for terahertz waveguiding. *Optics Express* **18**(1) (2011) 309-322.
17. C. Themistos B. M. A. Rahman, C. Markides, M. Uthman, A. Quadir, and N. Kejalakshmy, Characterization of graphene-based devices for THz systems. in *Terahertz Physics, Devices, and Systems VIII: Advanced Applications in Industry and Defense*, (SPIE, 2014).
18. O. Mitrofanov, R. James, F. A. Fernández, T. K. Mavrogordatos, and J. A. Harrington, Reducing transmission losses in hollow THz waveguides. *IEEE Trans. Terahertz Science and Technol.* **1**(1) (2011) 124-132.

19. H. P. Uranus, H. J. W. M. Hoekstra, and E. van Groesen, Galerkin finite element scheme with Bayliss-Gunzburger-Turkel-like boundary conditions for vectorial optical mode solver. *J. Nonlinear Opt. Phys. and Mat.* **13**(2) (2004) 175-194.
20. H. P. Uranus and H. J. W. M. Hoekstra, Modelling of microstructured waveguides using a finite-element-based vectorial mode solver with transparent boundary conditions. *Optics Express* **12**(12) (2004) 2795-2809.
21. H. P. Uranus, H. J. W. M. Hoekstra, and E. van Groesen, Considerations on material composition for low-loss hollow-core integrated optical waveguides. *Optics Commun.* **260**(2) (2006) 577-582.
22. W. Wijaya and H. P. Uranus, Fabrication and characterization of all-plastic flexible microfluidic chip using thermal lamination of patterned sheet, in *Proc. The 4th Int. Conf. on Instrumentation, Communications, Information Technology, and Biomedical Engineering (ICICI-BME 2015)*, Bandung, Indonesia (2-3 Nov. 2015), pp. 254-259.
23. Tydex, Terahertz materials, www.tydex.ru.
24. J. S. Jin, G. J. Kim, and S. G. Jeon, Terahertz dielectric properties of polymers. *J. Korean Physical Soc.* **49**(2) (2006) 513-517.
25. M. Naftaly and R. E. Miles, Terahertz time domain spectroscopy for material characterizations. *Proc. of The IEEE* **95**(8) (2007) 1658-1665.
26. H. P. Uranus, Theoretical study on the multimodeness of the commercial endlessly single-mode PCF. *Opt. Commun.* **283**(23) (2010) 4649-4654.
27. Y. F. Zhu, M. Y. Chen, H. Wang, H. B. Yao, Y. K. Zhang, and J. C. Yang, Design and analysis of a low-loss suspended core terahertz fiber and its application to polarization splitter. *IEEE Photonics J.* **5**(6) (2013) 7101401.1-7101401.10.